Inverted band structure of type-III HgTe/$Hg_{1-x}Cd_xTe$ superlattices and its temperature dependence

C. R. Becker,* V. Latussek, G. Landwehr, and L. W. Molenkamp
Physikalisches Institut der Universität Würzburg, Am Hubland, 97074 Würzburg, Germany
(Received 22 January 2003; published 2 July 2003)

Intersubband transitions in (001)- and (112)B-orientated HgTe/$Hg_{1-x}Cd_xTe$ superlattices with an inverted band structure have been investigated in order to determine their band structure. The results are compared with $\boldsymbol{k}\cdot\boldsymbol{p}$ calculations in the envelope function approximation using the full 8×8 Kane Hamiltonian. Up to six intersubband transitions and their temperature dependences have been observed. Three transitions display a positive dependence on temperature and the remaining three a negative dependence. Agreement with theory for all observed transitions and both orientations is good. Due to the close proximity of the first conduction subband and the Fermi energy, the influence of the charge carriers must be taken into account.

DOI: 10.1103/PhysRevB.68.035202 PACS number(s): 78.20.Bh, 71.20.−b, 78.20.Ci

I. INTRODUCTION

As is well known the optical and magnetotransport properties of HgTe/$Hg_{1-x}Cd_xTe$ quantum wells (QW's) and superlattices (SL's) are determined by their band structure, which particularly in type-III superlattices is largely determined by that of the quantum well. This has been demonstrated for the optical properties of semiconducting superlattices with a normal band structure, i.e., with a quantum well width of $d_w \leqslant 6$ nm.[1,2] Recently large Rashba[3] spin-orbit (SO) splitting has been observed in *n*-type modulation-doped HgTe/$Hg_{1-x}Cd_xTe$ quantum wells with an inverted band structure, i.e., $d_w \geqslant 6$ nm, by means of Shubnikov–de Haas (SdH) oscillations.[4,5] Rashba SO splitting magnitudes of up to 17 meV in these QW's were shown by Zhang *et al.*[5] to be due to the heavy-hole nature of the conduction subband. The authors were able to quantatively describe the observed Rashba SO splitting by means of self-consistent Hartree calculations of the band structure based on an 8×8 $\boldsymbol{k}\cdot\boldsymbol{p}$ model. The valence-band structure has been the subject of investigations of mixed conductivity in HgTe/$Hg_{1-x}Cd_xTe$ multiple quantum wells and superlattices.[6,7] Ortner *et al.*[8] have recently investigated the valence-band structure via magnetotransport experiments on *p*-type modulation-doped HgTe/$Hg_{0.3}Cd_{0.7}Te(001)$ quantum wells and have demonstrated that QW's with an inverted band structure are indirect semiconductors; i.e., their valence band has a maximum at finite $\boldsymbol{k}_{\|}$.

However, a systematic study of the optical properties of HgTe/$Hg_{1-x}Cd_xTe$ quantum wells or superlattices with an inverted band structure has yet to be published. An investigation of the optical properties of HgTe/$Hg_{1-x}Cd_xTe$ SL's with normal band structure has led to information about the quantum-well material and valence-band discontinuity between barrier and well.[2] The temperature dependence of the intersubband transition energies is directly influenced by that of the band gap of HgTe, which has led to a determination of the negative band gap of HgTe at room temperature as well as the temperature dependence of the heavy-hole effective mass. Furthermore, it was demonstrated that the valence-band offset is to a good approximation primarily responsible for the energy difference between the first heavy-hole, $H1$, and the first light hole, $L1$, subband of a HgTe/$Hg_{1-x}Cd_xTe$ superlattice with normal band structure. This energy difference was shown to be nearly independent of other superlattice parameters and, consequently, has led to a precise determination of the valence-band offset between HgTe and CdTe, Λ.

In this article it will be shown that the optical properties and the corresponding inverted band structure of SL's can be equally well described by means of the parameters used in calculations for SL's with normal band structure. In the latter case the band structure and consequently the optical properties strongly depend on the quantum well width, whereas this dependence is less pronounced for the former case.

II. EXPERIMENTAL DETAILS

Epitaxial growth was carried out in a Riber 2300, molecular beam epitaxial (MBE) system which has been modified to permit the growth of Hg-based materials as has been described elsewhere.[9] After the growth of a thin CdTe buffer layer, the HgTe/$Hg_{1-x}Cd_xTe$ superlattices were grown on (001)- and (112)B-oriented $Cd_{0.96}Zn_{0.04}Te$ substrates at 180 °C. The substrate temperature was determined with an accuracy of ±2 °C by means of a thermocouple which was in physical contact with a molybdenum substrate holder and was carefully calibrated at the melting points of indium and tin.

The composition of the barrier material has been determined by means of transmission measurements[10] on thick test layers of $Hg_{1-x}Cd_xTe$ grown under identical conditions with the exception of the absence of the HgTe layers. At a growth temperature of 180 °C, $x=0.70\pm0.02$ and $x=0.95\pm0.02$ for the (001) and (112)B orientations, respectively. The first value has been corroborated by a determination of the barrier TO phonon frequency for several (001) SL's.[11]

In this investigation the well thickness d_w and hence that of the barrier, d_b, of (001) superlattices have been deter-

mined by means of a dynamic simulation of the (002) and (004) Bragg reflections measured in a six-crystal x-ray diffractometer.[12,13] The intensity of the normally weak (002) Bragg reflection is about 15% of that of the (004) Bragg reflection in these superlattices. This is caused primarily by the HgTe layer: the structure factor for the (002) Bragg reflection is much larger for HgTe than for CdTe.[12] This is due to the larger Hg atom with its greater number of electrons.

X-ray diffraction in (112)B-oriented heterostructures is more complicated and the results are less accurate. First of all, there is only one useful reflection, (224), which is essentially equally strong for HgTe and CdTe. Second, shear strain results in a monoclinic distortion which must be taken into account before the data can be correctly simulated.[14,15]

Optical transmission measurements were carried out in the middle infrared regime with a Fourier transform spectrometer, Bruker IFS88. The lowest experimental frequency was limited by absorption due to multiple-phonon processes in the substrate and SL as well as the transmission of the optical windows in the cryostat. A $LiTaO_3$ detector was usually employed rather than a liquid-nitrogen-cooled detector—e.g., $Hg_{1-x}Cd_xTe$—because of its better linearity. The absorption coefficient was determined by fitting the experimental transmission spectra to a theoretical description of the multilayer system using standard matrix procedures.[16]

The position of the absorption edge was determined relative to that of the corresponding intersubband transition energy; the transition energies were calculated and the shape of the theoretical absorption coefficient was adapted to that of the experimental coefficient. Employment of a Gaussian distribution of either the quantum well and barrier widths or the composition of the wells results in good agreement with experiment. In general, absorption edges, defined by the corresponding maxima in the first derivative of the absorption coefficient, agree well with the intersubband transition energies with the exception of transitions which are not completely resolved. Hence we can confidently assign intersubband transition energies to the corresponding maxima in the first derivative.

It has been demonstrated that the absorption edges can also be determined from the transmission spectra directly.[2] If a transmission spectrum at one temperature is divided by a spectrum at a slightly different temperature, the result is proportional to the corresponding change in the absorption coefficient:

$$\frac{\Delta \mathrm{T}}{\mathrm{T}} \approx d \Delta \alpha, \tag{1}$$

where T and d are the transmission and sample thickness, respectively. Hence a good approximation of $\Delta\alpha$ can be obtained merely from a ratio of the transmission spectra[2] without the complications and uncertainties in calculating the absorption spectrum of the SL in a multilayer structure.[16] By keeping the temperature difference small, $\Delta T = 10$–40 K, residual interference effects are effectively reduced near the transition itself and nearly eliminated at other frequencies. The index of refraction undergoes a change of up to about 5%–10% near an intersubband transition; however, this has been shown to result in a negligible shift of the experimental absorption edge of $\leqslant 1$ meV.[2]

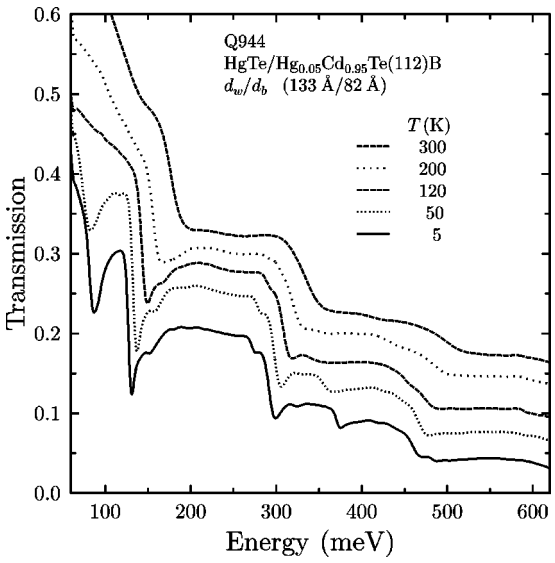

FIG. 1. The transmission spectra of a HgTe/$Hg_{0.05}Cd_{0.95}Te$(112)B superlattice, Q944, at several temperatures. The spectra are shifted along the vertical axis for clarity.

The transmission spectra of the SL's were measured at various temperatures; see, for example, Fig. 1. This was done for temperatures of 5–320 K with a temperature interval of 5 K at low temperatures and 10 K at higher temperatures, in order to improve the statistical significance of the data.

III. THEORETICAL DETAILS

Numerous $\boldsymbol{k}\cdot\boldsymbol{p}$ band structure calculations using the envelope function approximation for the HgTe/$Hg_{1-x}Cd_xTe$ superlattice have been published.[17–20] A brief review of the these calculations can be found in Ref. 2

In this investigation the bands of both bulk HgTe and CdTe are described by Kane's four-band model (8×8 $\boldsymbol{k}\cdot\boldsymbol{p}$) including all second-order remote band contributions. The envelope function method in the axial approximation has been employed to calculate the band structure of the HgTe/CdTe SL.[17,18] The axial approximation gives exact results for the band gaps of (001)-oriented systems, because nonaxial terms in the Hamiltonian vanish for $\boldsymbol{k}_\parallel = 0$; however, it is well known that the axial approximation is not exact for growth directions other than [001] and [111] even for $\boldsymbol{k}_\parallel = 0$.[21] Therefore we have taken the approach of Los *et al.*[22] and transformed the Hamiltonian into symmetry-adapted basis functions for the [112] growth direction. The band structure using this adapted Hamiltonian has been compared with an axial approximation for the [112] direction. The results of the axial approximation are not exact; however, they give a good approximation, within 1 or 2 meV, for the subband energies at $\boldsymbol{k}_\parallel = 0$ as well as for an average of the subband dispersion over all $\boldsymbol{k}_\parallel$ directions. Consequently, in order to reduce the calculation time, all absorption coefficient calculations and most intersubband transition energy

calculations were carried out using this adapted Hamiltonian in the axial approximation.

The effects of strain due to lattice mismatch were also taken into consideration, even though the lattice mismatch between HgTe and the $Hg_{1-x}Cd_xTe$ barriers is less than 0.1%. This results in a shift in intersubband transition energies of less then 3 meV and can therefore be neglected. In contrast to the [001] direction,[19] the strain tensor for the [112] direction has a shear strain component. This results in a piezoelectric field in the growth direction.[23] The strains for a free-standing, strained (112)B SL and a fully strained (112)B SL on a $Cd_{0.96}Zn_{0.04}Te$ substrate have been calculated. Due to the lack of a substrate in the former case, the shear strain component between the SL and its environment is zero. From these results the piezoelectric field has been calculated to be less than 5 mV/100 Å whose influence on intersubband transition energies is less than 1 meV and can therefore be neglected in the calculations.

A revised set of values for the band parameters deduced from measurements on bulk HgTe and $Hg_{1-x}Cd_xTe$ by Weiler[24] was employed which nevertheless reproduces the same bulk band structure ($\Delta=1.0$ eV, $\gamma_1=4.1$, $\gamma_2=0.5$, $\gamma_3=1.3$, $F=0$, and $E_p=18.8$ eV). Since the SL band structure is primarily determined by that of the quantum well and is influenced to a much lesser degree by the band structure of the barrier, the above values were employed for both the HgTe quantum wells and the $Hg_{1-x}Cd_xTe$ barriers. This results in no significant changes in the calculated band structure. According to Weiler[24] the only parameter that changes significantly with alloy composition and temperature is the energy gap. The energy gaps of HgTe and $Hg_{1-x}Cd_xTe$ were taken from a slight alteration of the empirical $E_g(x,T)$ relationship according to Laurenti *et al.*,[10] which takes a recently determined value for HgTe at room temperature into account.[2] The valence-band offset between HgTe and CdTe was taken to be

$$\Lambda(T)=\Lambda_0+\frac{d\Lambda}{dT}T \tag{2}$$

where $\Lambda_0=570$ meV and $d\Lambda/dT=-0.40$ meV/K according to Becker *et al.*[2] and $\Lambda(T)$ is assumed to vary linearly with x for $Hg_{1-x}Cd_xTe$, i.e., $x\Lambda(T)$.[25] An interface width which results during growth or from interdiffusion of the two types of layers was integrated into the theory. The concentration profile across the interface is described by an error function similar to an experimental profile according to Kim *et al.*[26]

The complex dielectric constant can be written as

$$\varepsilon(\omega)=\varepsilon_R(\omega)+i\frac{\sigma(\omega)}{\omega\epsilon_0}, \tag{3}$$

where $\varepsilon_R(\omega)$ is the residual contribution of the lattice and higher subbands which is assumed to be constant over the frequencies of interest in this investigation, $\varepsilon_R(\omega)\approx 10$. The complex dynamic conductivity $\sigma(\omega)$ is determined by making use of Kubo's formula,[27] and finally the absorption coefficient is given by

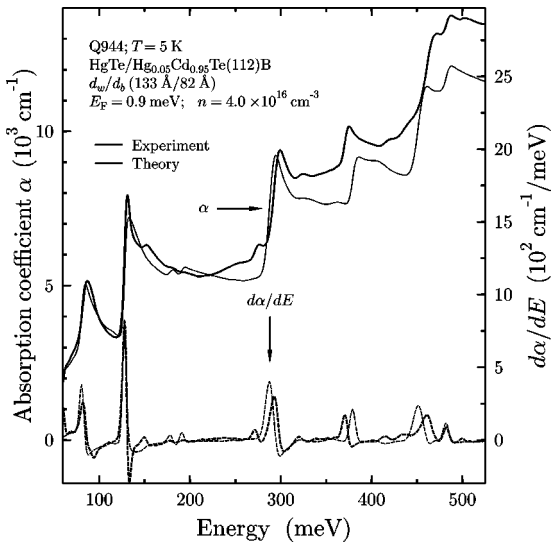

FIG. 2. The experimental (thick line) and theoretical (thin line) absorption coefficients and their first derivatives (thick and thin dashed lines, respectively) for a HgTe/$Hg_{0.05}Cd_{0.95}Te$(112)B SL, Q944, at 5 K.

$$\alpha(\omega)=\frac{\omega}{c}\frac{\sqrt{2}\varepsilon_2(\omega)}{\sqrt{\varepsilon_1(\omega)+|\varepsilon(\omega)|}}, \tag{4}$$

where $\varepsilon_1(\omega)$ and $\varepsilon_2(\omega)$ are the real and imaginary components of $\varepsilon(\omega)$, respectively.

IV. RESULTS AND DISCUSSION

A. (112)B orientation

Transmission spectra of an (112)B-oriented SL are shown in Fig. 1 at several temperatures. Numerous distinctive steps are visible, which with decreasing temperature become more pronounced. The three broad steps at 300 K have been assigned to the $H2$-$E2$, $H3$-$E3$, and $H4$-$E4$ intersubband transitions. H, L, and E are the heavy-hole, light-hole, and electron subbands, respectively. In the inverted band regime the valence subbands and the conduction subbands at low energies are mixed to varying degrees at finite $\boldsymbol{k}$; however, for the sake of brevity we shall continue to use these designations. With decreasing temperature fine structure becomes readily discernable: at lower temperatures numerous minima are visible and noteworthy are the pronounced minima at the band edges near 128 and 288 meV, a feature which is normally associated with an exciton. The absorption spectrum together with the first derivative of the absorption coefficient for this SL at 5 K is shown in Fig. 2. At least three additional peaks at approximately 80, 368, and 482 meV are now visible which are assigned to the $E1$-$H1$, $L2$-$H1$, and $L2$-$E2$ intersubband transitions.

The calculated absorption coefficient spectrum, which is also shown in Fig. 2, is in good agreement with experiment. This agreement between the calculated transition probabilities and the observed absorption coefficient spectrum, as well as between the calculated and experimental frequencies, cor-

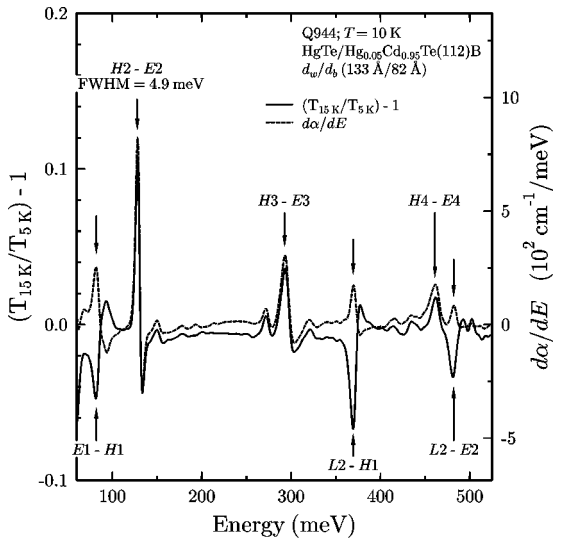

FIG. 3. The ratio of the transmission T at $T=15$ and $T=5$ K (solid line) is compared with the first derivative of α (dashed line) for Q944 at 10 K. The intersubband transitions are indicated by arrows. Minima are observed in the transmission ratio for those with a negative temperature dependence.

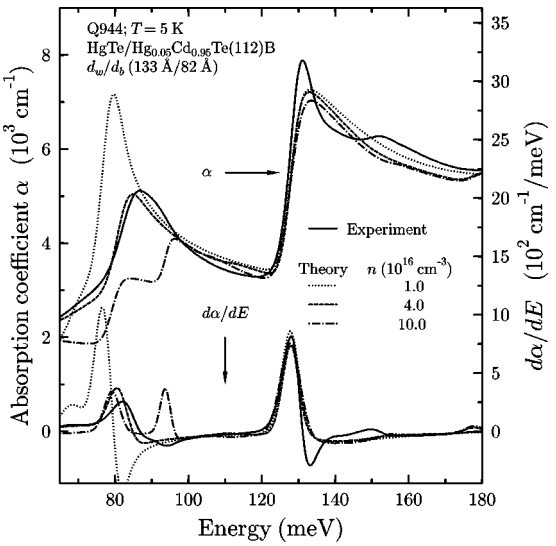

FIG. 4. The experimental (solid line) and theoretical (dotted, dashed, and dash-dotted lines) absorption coefficients and their first derivatives for a $HgTe/Hg_{0.05}Cd_{0.95}Te(112)B$ SL, Q944, for three different electron concentrations at 5 K.

raborates the above-mentioned assignments. The relative heights of the corresponding steps are in good agreement with experiment, even though the absolute magnitude of the absorption coefficient α is underestimated due to the neglect of Coulomb interaction between electron and hole.[28]

1. Intersubband transition energies

The absorption edges have been determined from both the transmission and absorption spectra. In the latter case, the absorption edge is defined as the energy at the maximum value of the first derivative of the absorption coefficient. This is schematically demonstrated in Fig. 2 for Q944 at 5 K. The full widths at half maximum (FWHM) of the derivative for the $E1$-$H1$ and $H2$-$E2$ transitions are 7.2 and 4.9 meV, respectively. Also shown are a theoretically calculated α and its derivative. The shape and width of the experimental α and $d\alpha/dE$ for Q944 in Fig. 2 were simulated by assuming a Gaussian distribution of quantum well widths with $\sigma = 4.0$ Å.[29] The absorption edges coincide with the intersubband transition energies of $H2$-$E2$ to within ± 2 meV for all samples. The agreement for most of the other transitions is not as good due to their close proximity, e.g., $H4$-$E4$ and $L2$-$E2$, as well as due to the influence of the Fermi energy on some intersubband transitions as discused below.

With the other method the absorption edge is determined from the change in the absorption coefficient according to Eq. (1). The near equivalence of these two methods of determining the band edges and consequently the intersubband transition energies is demonstrated in Fig. 3. In this figure the dashed line represents $d\alpha/dE$ at 10 K and the solid line represents $T_{15\,K}/T_{5\,K}-1$ whose effective temperature is also 10 K. The experimental transition energies defined as the energies at the maximum or minimum values of $T_{15\,K}/T_{5\,K}-1$ are in good agreement with the corresponding energies for $d\alpha/dE$; i.e., the energy difference is $\leqslant 1$ meV for all six transitions. Because the $E1$-$H1$, $L2$-$H1$, and $L2$-$E2$ intersubband transitions are negatively dependent on temperature, minima in $T_{15\,K}/T_{5\,K}-1$ are observed instead of the maxima for the other three intersubband transitions.

Because the Fermi energy is close to the $H1$ subband and strongly depends on the charge carrier concentration due to the small effective electron mass, the $E1$-$H1$ and $L2$-$H1$ intersubband transitions are influenced by the electron density n. This is illustrated for $E1$-$H1$ in Fig. 4 in which the theoretical α for three values of n is plotted together with the experimental absorption coefficient. At low carrier densities one sharp peak in $d\alpha/dE$ is visible, which with increasing densities shifts to higher energies and becomes broader. Finally, at higher carrier concentrations, two broad steps are expected. The higher-energy feature is due to the Burstein-Moss[30] shifted $E1$-$H1$ intersubband transition, whereas the expected lower-energy feature is a result of the $H4$-$H1$ transition. These two intersubband transitions at different carrier densities are schmatically shown as arrows in a diagram of the band structure dispersion shown in Fig. 5. The transition probability of the $H4$-$H1$ transition at low densities, i.e., at $\boldsymbol{k}\approx 0$, is negligible but is finite for $\boldsymbol{k}>0$, according to the calculated dipole matrix elements shown in Fig. 6.

In addition the $L2$-$H1$ intersubband transition also shifts to higher energies with increasing n. Therefore these results indicate that a rough estimate of n can be obtained from transmission measurements.

2. Temperature dependence

The intersubband transition energies for Q944 are shown as a function of temperature in Fig. 7. Values determined from the transmission ratio are indicated by solid circles and

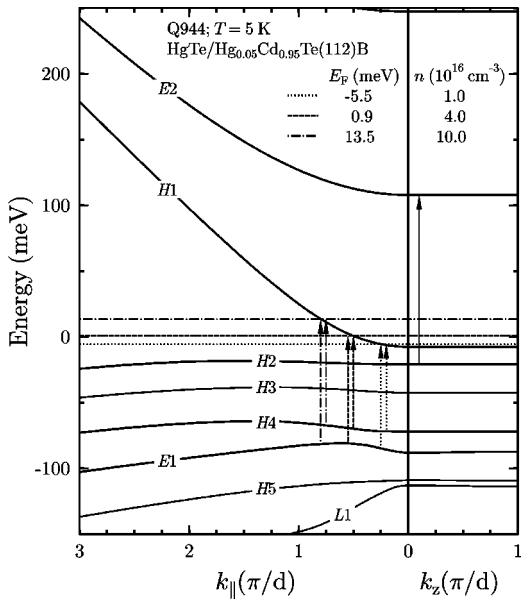

FIG. 5. The band structure dispersion for a HgTe/$Hg_{0.05}Cd_{0.95}$Te(112)B SL, Q944, at 5 K. The intersubband transitions; $E1$-$H1$, $H4$-$H1$, and $H2$-$E2$; are indicated by arrows for three different Fermi energies, i.e., electron concentrations, at 5 K.

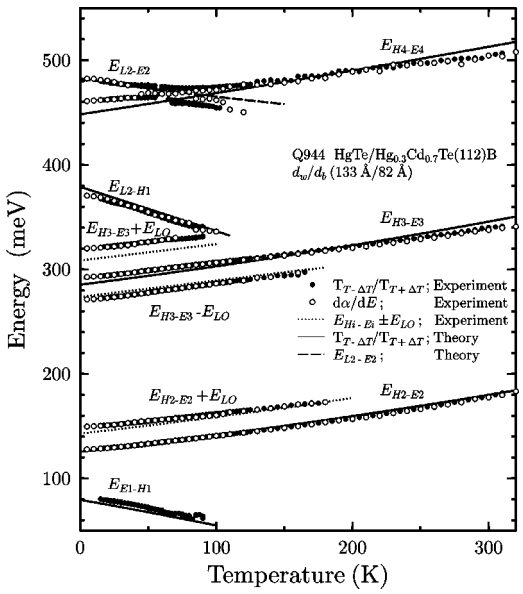

FIG. 7. Experimental values of the observed intersubband transitions from $d\alpha/dE$ (open circles) and $T_{T+\Delta T}/T_{T-\Delta T}$ (solid circles) together with theoretical results (lines) for a HgTe/$Hg_{0.05}Cd_{0.95}$Te(112)B SL, Q944, as a function of temperature.

those from $d\alpha/dE$ by open circles. The energies from these two methods are nearly equal: most of the former symbols are obscured by the latter. As can be seen there is less scatter in the data from the transmission ratio method. The experimental values of the $H2$-$E2$, $H3$-$E3$, and $H4$-$E4$ intersubband transition energies display a significant positive temperature dependence. In contrast, the temperature dependence of the $E1$-$H1$, $L2$-$H1$, and $L2$-$E2$ transition energies is negative. The temperature dependence of the initial subband is less than that of the final subband for $H2$-$E2$, $H3$-$E3$, and $H4$-$E4$ and vice versa for the other three intersubband transitions. Noteworthy are the weaker features in Fig. 7, whose temperature dependence is similar to that of the neighboring $H2$-$E2$ and $H3$-$E3$ intersubband transitions. In addition their energies are approximately equal to that of the respective transitions plus or minus the LO phonon energy, $E_{LO} \approx 17$ meV, of HgTe.[31] The agreement for $E_{H3\text{-}E3} + E_{LO}$ is not as good, due to the resonance induced minimum on the high-frequency side of $H3$-$E3$.

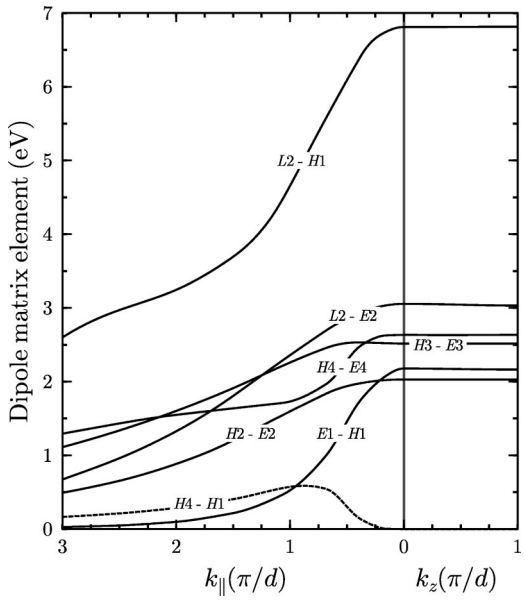

FIG. 6. The dipole matrix elements for a HgTe/$Hg_{0.05}Cd_{0.95}$Te(112)B SL, Q944, at 5 K.

Using the temperature dependence of the valence-band offset, the HgTe band gap, and the heavy-hole effective mass according to Becker *et al.*,[2] the temperature dependence of the six primary transitions from the initial subband i to the final subband j have been calculated:

$$\frac{dE_{i-j}}{dT} = f\left(\frac{dE_g(\mathrm{HgTe},T)}{dT},\ \frac{d\Lambda}{dT},\ \frac{m^*_{hh}}{dT}\right). \tag{5}$$

The theoretical intersubband transition energies have been determined from the ratio of the calculated transmission via Eq. (1), with the exception of energies of an unresolved transition, i.e., $L2$-$E2$, which have been determined from the band structure. All values are plotted together with the experimental results in Fig. 7 and are obviously in good agreement with the experimental values. The agreement is excellent for $H2$-$E2$, but is not as good for transitions at progressively higher energies as expected for a perturbation theory or for unresolved transitions.

B. (001) orientation

This more symmetric surface has a number of advantages but also distinct disadvantages. For example, the more symmetric Hamiltonian does not lead to a monoclinic distortion or a piezoelectric effect as is the case for (112).[14,15] As mentioned above, values for the well and barrier widths via x-ray

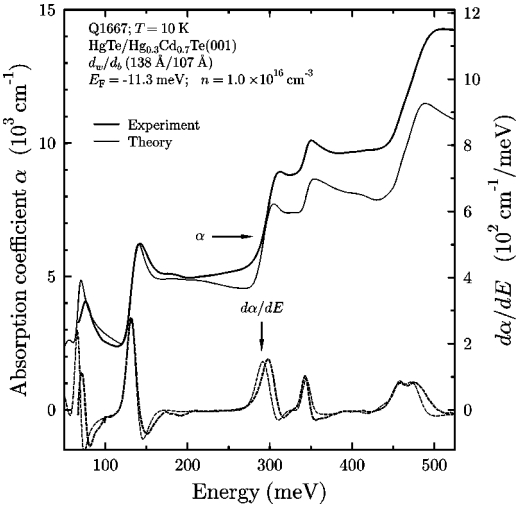

FIG. 8. The experimental (thick line) and theoretical (thin line) absorption coefficients and their first derivatives (thick and thin dashed lines, respectively) for a HgTe/$Hg_{0.3}Cd_{0.7}$Te(001) SL, Q1667, at 10 K.

diffraction are more accurate; however, the Cd concentration in the barriers is appreciably lower, 0.70 instead of 0.95. This has an important consequence. The absorption edges are up to a factor of 2.5 broader, apparently due to greater alloy fluctations in the barriers.[29]

The experimental and theoretical absorption coefficients and their derivatives for a (001) SL, Q1667, at 10 K are plotted in Fig. 8. Agreement between experiment and theory is good, as is the case for the (112)B-orientated SL, Q944, and for two additional (001)-oriented SL's not shown here. Because the band structure for these two orientations is similar, the $E1$-$H1$ and $L2$-$H1$ intersubband transitions are also strongly influenced by the electron density for the (001) orientation. This is illustrated for $E1$-$H1$ in Fig. 9 in which the

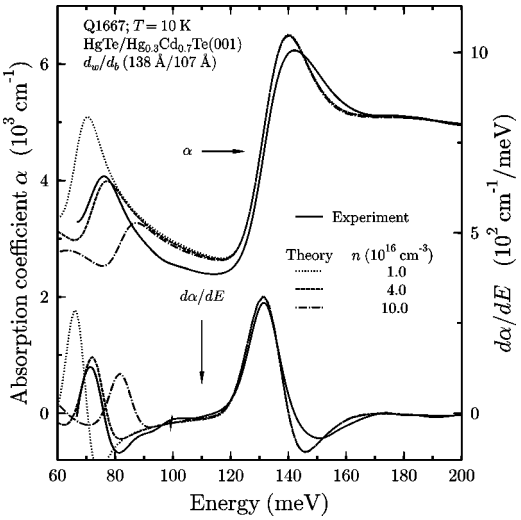

FIG. 9. The experimental (solid line) and theoretical (dotted, dashed, and dash-dotted lines) absorption coefficients and their first derivatives for a HgTe/$Hg_{0.3}Cd_{0.7}$Te(001) SL, Q1667, for three different electron concentrations at 10 K.

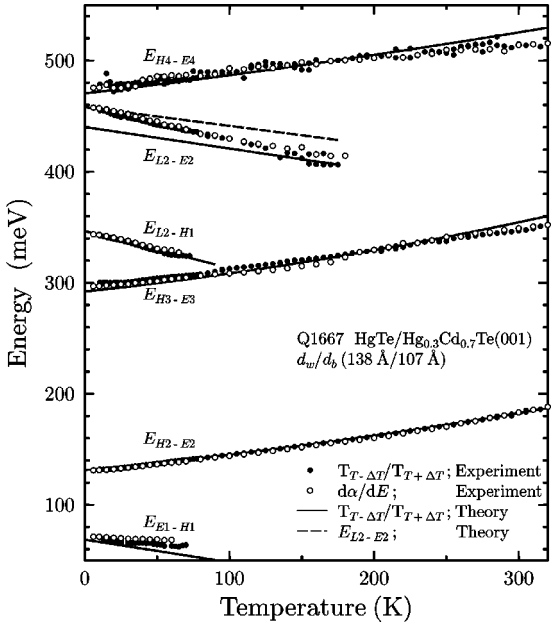

FIG. 10. Experimental values of the intersubband transition energies from the maximum value of $d\alpha/dE$ (open circles) and the ratio of the transmission spectra ($T_{T+\Delta T}/T_{T-\Delta T}$, solid circles), together with theoretical results (lines) for a HgTe/$Hg_{0.3}Cd_{0.7}$Te(001) SL, Q1667, vs temperature.

theoretical α for three values of n are plotted together with the experimental absorption coefficient. The sharp peak in $d\alpha/dE$ at low carrier densities shifts to higher energies and becomes broader with increasing densities. And as is the case for Q944, two broad steps are expected at higher carrier concentrations, which are due to the Burstein-Moss[30] shifted $E1$-$H1$ intersubband transition and the $H4$-$H1$ transition for $\boldsymbol{k}>0$. Again demonstrating that a rough estimate of n can be obtained from transmission measurements.

The intersubband transition energies for Q1667 are plotted as a function of temperature in Fig. 10. Results from the transmission ratio method are represented by solid circles and those from $d\alpha/dE$ by open circles. Here these two methods are also nearly equivalent and there is less scatter in the data from the transmission ratio method. Since features in α are much less pronounced in the (001)-oriented SL's, the transitions involving the LO phonon were not observed. The calculated temperature dependence of the observed intersubband transitions, which are displayed as lines in Fig. 10, is obviously in good agreement with the experimental values. As can be seen, agreement is better for transitions at lower energies, especially for $H2$-$E2$, as is expected for a perturbation theory.

V. CONCLUSIONS

Intersubband transitions and their dependence on temperature in semiconducting HgTe/$Hg_{1-x}Cd_xTe$ superlattices with an inverted band structure have been investigated for the (001) and (112)B orientations. $\boldsymbol{k}\cdot\boldsymbol{p}$ calculations in the envelope function approximation using the full 8×8 Kane Hamiltonian are in good agreement with experiment. Re-

cently published values for $\Lambda(T)$, $E_g(\mathrm{HgTe},T)$, and m_{hh}^* from an investigation of $HgTe/Hg_{1-x}Cd_xTe$ superlattices with a normal band structure have been employed. Of the six observed intersubband transitions, the temperature dependences of three are positive and those of the other three are negative. Transitions have been observed in a (112)B-oriented SL, which involve the $H2$-$E2$ and $H3$-$E3$ intersubband transitions, and the LO phonon. Furthermore, the charge carrier density strongly influences the $E1$-$H1$ and $L2$-$H1$ intersubband transitions. Hence a rough estimate of n can be determined from the optical absorption.

ACKNOWLEDGMENTS

The support of the Deutsche Forschungsgemeinschaft via SFB 410, II-VI Halbleiter: Wachstumsmechanismen, niederdimensionale Strukturen und Grenzflächen, is gratefully acknowledged.

*Electronic address: becker@physik.uni-wuerzburg.de

[1] J. R. Meyer, C. A. Hoffman, T. H. Myers, and N. C. Giles, in *Handbook on Semiconductors*, edited by T. S. Moss, Vol. 3 edited by S. Mahajan (North-Holland, Amsterdam, 1994), p. 535.

[2] C. R. Becker, V. Latussek, A. Pfeuffer-Jeschke, G. Landwehr, and L. W. Molenkamp, Phys. Rev. B **62**, 10 353 (2000).

[3] E. I. Rashba, Fiz. Tverd. Tela **2**, 1224 (1960) [Sov. Phys. Solid State **2**, 1109 (1960)]; Yu. A. Bychkov and E. I. Rashba, Pis'ma Zh. Éksp. Teor. Fiz. **39**, 66 (1984) [JETP Lett. **39**, 78 (1984)].

[4] M. Schultz, F. Heinrichs, U. Merkt, T. Colin, T. Skauli, and S. Løvold, Semicond. Sci. Technol. **11**, 1168 (1996).

[5] X. C. Zhang, A. Pfeuffer-Jeschke, K. Ortner, V. Hock, H. Buhmann, C. R. Becker, and G. Landwehr, Phys. Rev. B **63**, 245305 (2001).

[6] C. A. Hoffman, J. R. Meyer, F. J. Bartoli, J. W. Han, J. W. Cook, J. F. Schetzina, and J. N. Schulman, Phys. Rev. B **39**, 5208 (1989).

[7] J. R. Meyer, C. A. Hoffman, and F. J. Bartoli, Physica B **191**, 171 (1993), and references therein.

[8] K. Ortner, X. C. Zhang, A. Pfeuffer-Jeschke, C. R. Becker, G. Landwehr, and L. W. Molenkamp, Phys. Rev. B **66**, 075322 (2002).

[9] C. R. Becker, V. Latussek, W. Spahn, F. Goschenhofer, S. Oehling and G. Landwehr, in *Growth and Characterization of Materials for Infrared Detectors*, edited by R. E. Longshore and J. W. Baars [Proc. SPIE **2554**, 6 (1995)].

[10] J. P. Laurenti, J. Camassel, A. Bouhemadou, B. Toulouse, R. Legros, and A. Lusson, J. Appl. Phys. **67**, 6454 (1990).

[11] M. von Truchsess, V. Latussek, F. Goschenhofer, C. R. Becker, G. Landwehr, E. Batke, R. Sizmann, and P. Helgesen, Phys. Rev. B **51**, 17 618 (1995).

[12] M. Möller, R. N. Bicknell-Tassius, and G. Landwehr, J. Appl. Phys. **72**, 5108 (1992).

[13] C. R. Becker, L. He, M. M. Regnet, M. M. Kraus, Y. S. Wu, G. Landwehr, X. F. Zhang, and H. Zhang, J. Appl. Phys. **74**, 2486 (1993).

[14] M. Li, C. R. Becker, R. Gall, W. Faschinger, and G. Landwehr, Appl. Phys. Lett. **71**, 1822 (1997).

[15] M. Li, R. Gall, C. R. Becker, T. Gerhard, W. Faschinger, and G. Landwehr, J. Appl. Phys. **82**, 4860 (1997).

[16] D. Fasold, K. Heil, and S. Jetschke, Phys. Status Solidi A **86**, 125 (1984).

[17] L. R. Ram-Mohan, K. H. Yoo, and R. L. Aggarwal, Phys. Rev. B **38**, 6151 (1988).

[18] N. F. Johnson, H. Ehrenreich, P. M. Hui, and P. M. Young, Phys. Rev. B **41**, 3655 (1990).

[19] A. Simon, D. Bertho, D. Boiron, and C. Jouanin, Phys. Rev. B **42**, 5221 (1990).

[20] J. R. Meyer, C. A. Hoffman, and F. J. Bartoli, Semicond. Sci. Technol. **5**, S90 (1990).

[21] R. Winkler and A. I. Nesvizhskii, Phys. Rev. B **53**, 9984 (1996).

[22] J. Los, A. Fasolino, and A. Catellani, Phys. Rev. B **53**, 4630 (1996).

[23] Liberato De Caro and Leander Tapfer, Phys. Rev. B **51**, 4374 (1995).

[24] M. H. Weiler, in *Semiconductors and Semimetals*, edited by R. Willardson and A. C. Beer (Academic Press, New York, 1981), Vol. 16, p. 119.

[25] C. K. Shih and W. E. Spicer, Phys. Rev. Lett. **58**, 2594 (1987).

[26] Y. Kim, A. Ourmazd, M. Bode, and R. D. Feldman, Phys. Rev. Lett. **63**, 636 (1989).

[27] E. Bangert, P. Boege, V. Latussek, and G. Landwehr, Semicond. Sci. Technol. **8**, S99 (1993).

[28] Christian Tanguy, Phys. Rev. Lett. **75**, 4090 (1995), and references therein.

[29] C. R. Becker, A. Pfeuffer-Jeschke, V. Latussek, M. Li, K. Ortner, V. Daumer, S. Oehling, W. Tang, and G. Landwehr, J. Cryst. Growth **184/185**, 1185 (1998).

[30] E. Burstein, Phys. Rev. **93**, 632 (1954); T. S. Moss, Proc. Phys. Soc. London, Sect. B **76**, 775 (1954).

[31] R. Dornhaus and G. Nimtz, in *Narrow-Gap Semiconductors*, edited by G. Höhler and E. A. Niekisch (Springer-Verlag, Berlin, 1983), Vol. 98, p. 119.